THE JOURNAL OF PHYSICAL CHEMISTRY C

Article

pubs.acs.org/JPCC

# Nature of Absorption Bands in Oxygen-Functionalized Graphitic Carbon Dots

Mária Sudolská,[†] Matúš Dubecký,[†] Sunandan Sarkar,[†] Claas J. Reckmeier,[‡] Radek Zbořil,[†] Andrey L. Rogach,[‡] and Michal Otyepka*[,†]

[†]Regional Centre of Advanced Technologies and Materials, Department of Physical Chemistry, Faculty of Science, Palacký University Olomouc, Tř. 17. listopadu 12, 771 46 Olomouc, Czech Republic

[‡]Department of Physics and Materials Science and Centre for Functional Photonics, City University of Hong Kong, 83 Tat Chee Avenue, Hong Kong SAR, China

Supporting Information

**ABSTRACT:** Carbon dots (CDs) belong to a class of materials considered technologically important for their tunable absorption and emission properties and a huge application potential in cell labeling, theranostics, and optoelectronic technologies including LED diodes. Although improvement of their properties relies on a fundamental understanding of the underlying photophysical processes, this is currently far from complete. Here, we analyze the absorption spectra of nontrivial multilayer graphitic oxygen-functionalized CD models. The results suggested that the experimentally observed broad bands around 300 nm originated from n → $\pi^*$ and $\pi$ → $\pi^*$ charge transfer transitions, whereas the effects of structural/energetic disorder, water environment, deprotonation, and excitonic coupling only weakly contributed to the spectra when compared to their monolayer counterparts. Owing to their weak interlayer interactions and thermal accessibility of low-energy conformations, the graphitic CDs are prone to structural disorder and consequent spectral-line broadening.

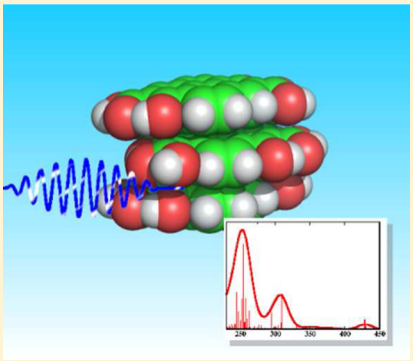

## INTRODUCTION

Carbon dots (CDs) are of broad scientific interest owing to their easy preparation, light weight, high stability and biocompatibility, and tunable properties, like size, absorption/emission characteristics, and easy modification of their composition and functionalization.[1−9] These properties predispose them for a large number of technological applications, ranging from bioimaging to modern visual technology.[10] Future development of CDs with improved properties relies on gaining a fundamental understanding of their structural features and absorption and emission properties, which is currently far from complete.

To date, only simplified single-layer models of CDs have been considered when modeling their absorption and/or emission spectra and effects of edge functionalization.[11−14] However, such models are not able to capture physical phenomena like effects of stacking, excitonic coupling, and/or interlayer charge transfer (i.e., electronic transitions involving different subsystems/layers within the stacked system[15,16]) that may strongly affect the optical properties of CDs. It is well established that functional groups present in the CD shell modulate their electronic structure and optical transitions,[11,12,17−19] but there is no general consensus regarding the fine interplay of these effects. Besides the well-established mesomeric and induction effects of functional groups, other effects, such as breakage of $\pi$-conjugation, stacking, protonation equilibria, and environment (i.e., presence of solvent, counterions, etc.), need to be taken into account.

Here, we introduce a simple multilayer model of a CD (∼1.2 nm in size) that qualitatively mimics the experimental absorption spectra and allows the nature of CD absorption bands to be deciphered. The effects of aqueous environment and deprotonation were also considered. The developed model included all important physical phenomena that may contribute to the optical properties of CDs but was small enough to be tractable by quantum chemistry methods, providing a key tool for obtaining the required information. Time-dependent density functional theory (TD-DFT) calculations showed that the low-energy absorption bands (>300 nm) generated by the model in both vacuum and solvent were dominated by interlayer charge transfer transitions of $\pi$ → $\pi^*$ nature (transitions from bonding $\pi$ orbitals to antibonding $\pi^*$ orbitals between different molecules or fragments within the same molecule), rather than exclusively n → $\pi^*$ (transitions from nonbonding orbitals—lone pairs—to $\pi^*$ antibonding orbitals, commonly weak due to symmetry reasons[15,16,20]), which are frequently assumed to take place in this spectral range.[21−24]

**Received:** April 29, 2015
**Revised:** May 13, 2015
**Published:** May 15, 2015





DOI: 10.1021/acs.jpcc.5b04080
J. Phys. Chem. C 2015, 119, 13369−13373

**Scheme 1. Considered Structures and Their Assembly to the Final Multilayer CD Model Studied in Vacuum (Bottom Panel) or a Water Phase (Top Panel)**

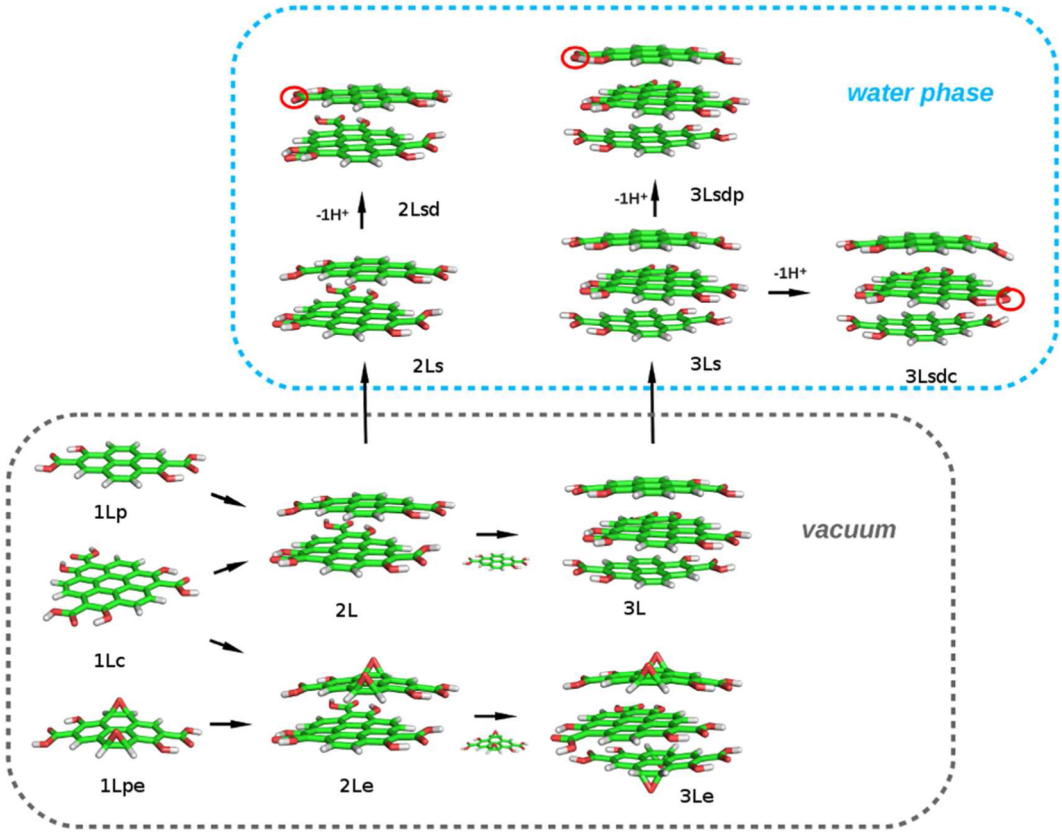


## COMPUTATIONAL DETAILS

All considered models (Scheme 1) were fully optimized within the Becke three-parameter hybrid density functional (B3LYP)[25] with the D3 empirical dispersion correction by Grimme et al.[26] and 6-31++G(d,p) Pople basis set. Genuine minima at the potential energy surface were confirmed by frequency calculations (for monolayer and bilayer complexes). Absorption spectra were computed within the TD-DFT framework with the range-separated hybrid $\omega$B97xD exchange-correlation functional[27] and 6-31+G(d) basis set on all atoms. This procedure (including structure optimization) has previously been confirmed to be acceptable for modeling of vertical absorption spectra including charge transfer transitions.[28−30] The effects of hydration were studied within the conductor-like polarizable continuum model (C-PCM).[31,32] Excitonic coupling was quantified according to Knippenberg et al.[33] Electron density differences were obtained by subtraction of total CI electron densities. The Gaussian G09 package[34] was used throughout the work.

The multilayer models (Scheme 1) were built from functionalized (−OH, −COOH, and C−O−C) pyrene and coronene based one-layer building blocks. These were preoptimized as single layers within the systematic energy-driven high-throughput combinatorial substitution search (more than 130 molecules were tested). The selected most stable single-layer structures involved local neighboring −OH/−COOH hydrogen-bonded pairs. Multiples of such pairs were found to prefer distant occupations. For example, in the case of pyrene, two COOH groups were found to prefer positions 2 and 7, while OH groups resided nearby at positions 1 and 6. Two epoxy groups in pyrene were found to prefer positions 4 and 5, and 9 and 10. The stacked systems revealed slight bending at the edges with −COOH and −OH groups inclined toward each other. Optimizations in solvent (i.e., water) and additional deprotonation did not result in qualitatively significant geometry changes with respect to the gas phase structures. Since inhomogeneity and complexity of CDs implies the presence of structural and/or energetic disorder, i.e., not only the lowest-energy structures/configurations are effectively present in the measured ensembles, the robustness of spectra was tested by comparison of five conformations of the 2L complex (Supporting Information Figure S4). The test revealed only weak dependence on the overall features, and thus only the low energy structures were considered throughout the work.

## RESULTS AND DISCUSSION

CDs have complex structures comprising a graphitic (or amorphous) core and a shell,[35] which bears various edge and in-plane functional groups containing oxygen, nitrogen, sulfur, and possibly other heteroatoms.[19,36,37] In this work, graphitic CDs containing oxygen functional groups (hydroxyl, carboxyl, and epoxy) were studied. In order to provide a simple but qualitatively correct structural CD model, we started with an assembly of multiple stacked bi- and trilayer complexes constructed from simple functionalized pyrene- and coronene-based building blocks identified from an energy-driven combinatorial search (see Computational Details section). The final CD model system was selected by qualitative matching of the calculated vs experimental absorption spectra that typically


DOI: 10.1021/acs.jpcc.5b04080
J. Phys. Chem. C 2015, 119, 13369−13373

reveal a broad shape with only a few structureless peaks (see, e.g., refs 38−40).

A three-layer CD model (3L, Scheme 1) was constructed, consisting of one central coronene-based unit (1Lc, Scheme 1) and two surface pyrene-based units (1Lp, Scheme 1). The CD had a size of approximately 1.2 × 1.2 nm, height of ∼0.9 nm, and interlayer spacing of ∼0.34 nm, similar to the interlayer spacing of graphite (0.334 nm).[41] Its broad spectrum (Figure 1) was dominated by an interlayer charge transfer $\pi \rightarrow \pi^*$ band

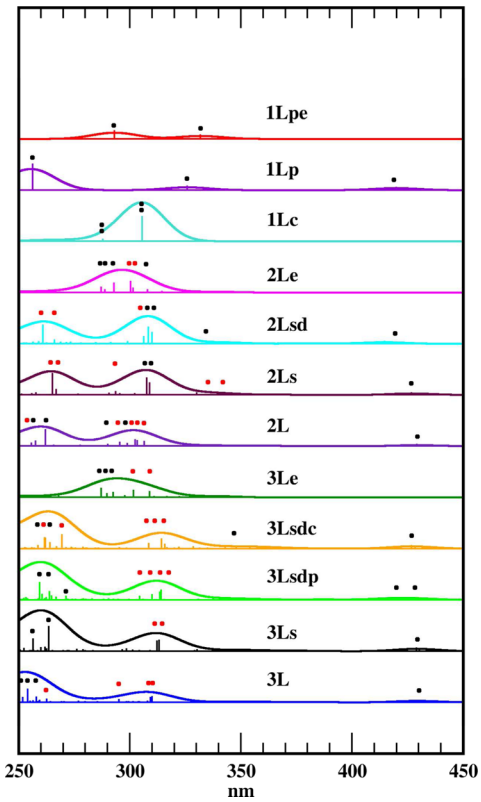


**Figure 1.** Calculated absorption spectra for the considered models (cf. Scheme 1). The indicated transitions (oscillator strength >0.1; black/red dots) are dominated by $\pi \rightarrow \pi^*$ character. Transitions with a significant charge transfer component are indicated by red.

centered at around 300 nm and more intense band at around 250 nm of $\pi \rightarrow \pi^*$ nature, for which the lowest intensity peak included a charge transfer component (Figure 2). It should be emphasized that the band centered at around 300 nm has been traditionally assigned to a n $\rightarrow \pi^*$ transition,[6,21,24] whereas the assignment of the transitions centered at around 250 nm is in accord with the available literature.[10]

Immersion of the 3L CD in a water environment (3Ls) caused a slight red-shift of the whole spectrum envelope

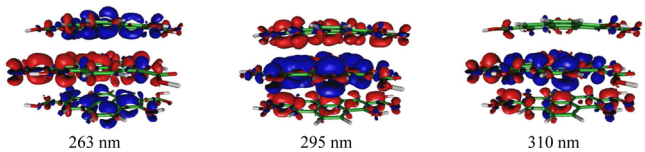


**Figure 2.** Electron density differences between the ground and excited states for the intense transitions in 3L (cf. Figure 1). Charge depletion and charge accumulation areas are indicated in blue and red, respectively.

(Figure 1). The charge transfer $\pi \rightarrow \pi^*$ transitions were shifted to higher wavelengths by ∼3−4 nm, and the center of the more intense band was also shifted in the same direction (by ∼5−6 nm) in qualitative agreement with a previous theoretical study on single-layer systems.[12] Deprotonation of the surface or middle layer of the 3Ls system (3Lsdp or 3Lsdc) did not induce any apparent qualitative change in the overall shape of the spectral envelopes when compared to 3Ls, even though some internal reshuffling of the discrete transitions took place. Our results also indicated that single-proton deprotonation would not be detectable by experiment. We note in passing that conclusions similar to the three-layer sequence 3L−3Ls−3Lsd(p/c) would also apply for the two-layer sequence 2L−2Ls−2Lsd.

As 3L consists of one 1Lc and two 1Lp subunits and may also be viewed as composed of the 2L and 1Lp systems, a detailed understanding of the constituent spectra (1Lp, 1Lc, 2L) may shed light on the origin of the individual peaks in the spectrum of 3L. Therefore, further discussion of the absorption spectra of the modeled systems is presented below in a bottom-up manner.

The spectra of the "one-layer" molecules (1Lp, 1Lc, Scheme 1) were characterized by discrete $\pi \rightarrow \pi^*$ bands over the whole spectral region (Figure 1). The 1Lp complex displayed a dominant transition at 256 nm and two weaker ones at 326 and 420 nm. The 1Lc spectrum showed a strong wide band at around 300 nm with two twofold degenerate $\pi \rightarrow \pi^*$ transitions at 305 and 288 nm. In the molecular orbital picture used, no pure n $\rightarrow \pi^*$ transitions were found in the spectra because the oxygen lone pair orbitals hybridized with the pyrene $\pi$ cloud (see Figure S1 in the Supporting Information).

The stacking of the 1Lp and 1Lc monolayers led to 2L assembly (Scheme 1) stabilized by −29.2 kcal/mol (for more details, see Supporting Information Table S1) and emergence of interlayer charge transfer transitions in the low-energy region around 300 nm (2L, Figure 1), which cannot be viewed as pure $\pi \rightarrow \pi^*$ nor n $\rightarrow \pi^*$ nature due to weak mixing of the orbital character. The most intense peak at 262 nm was dominated by transition within the 1Lp layer (Supporting Information Figure S2). Further inspection of the 2L spectra revealed only weak sensitivity to the structural changes (the relative energies for five additional conformations are reported in Supporting Information Figure S4). On the other hand, since the relative energies of the low-energy conformations reached up to a few kcal/mol, structural disorder and consequent line-broadening would be present at finite temperature due to their thermal accessibility.

In order to quantify excitonic coupling and understand the nature of peak-shifts and variation of oscillator strengths at a qualitative level, we used the 2L model for a rigid scan of the interlayer distance between its monolayer 1Lc and 1Lp constituents. Absorption spectra were calculated for each distance, as shown in Supporting Information Figure S5. We found that at the separation of 5 Å, i.e., in a distant case, the spectrum appears as a sum of (structurally distorted) isolated 1Lc and 1Lp spectra (Supporting Information Figure S5); i.e., no artificial charge transfer occurs. The equilibrium spectrum of 2L complex resembles the distant case well, which is indicative of weak transition dipole coupling in 2L complex. For the two degenerate pairs of selected peaks, as indicated in Supporting Information Figure S5, we extrapolated the Förster coupling to the equilibrium distance (Supporting Information Figure S6). The estimated coupling reveals only small values of about 550


DOI: 10.1021/acs.jpcc.5b04080
J. Phys. Chem. C 2015, 119, 13369−13373

and 240 $cm^{-1}$ respectively (for more details, see Supporting Information).

The 3L system contained an additional 1Lp layer compared to the 2L system (stabilization energy −27.8 kcal/mol, the total stabilization energy −57.0 kcal/mol), which resulted in further orbital mixing (with respect to 2L), preventing mapping of peaks to the spectra of its constituents. For example, the most intense peak (254 nm) of the 3L spectrum was of $\pi \rightarrow \pi^*$ nature. But, since the orbitals participating in this most intense transition were themselves mixtures of the original 1Lp and 1Lc orbitals (or 1Lp and 2L ones), no unambiguous assignment was possible.

The presence of surface epoxy groups in the one-layer 1Lpe model led to strong shifts in the absorption spectrum compared to the case of 1Lp. The first weak HOMO−LUMO transition of $\pi \rightarrow \pi^*$ nature was blue-shifted from 420 to 332 nm and its intensity increased (from 0.16 to 0.22), whereas the most intense peak in 1Lp (256 nm) was significantly red-shifted to 293 nm with simultaneously decreased relative intensity (from 1.55 to 0.48). We noted that in 1Lpe, the HOMO and LUMO were very similar in shape to those of 1Lp except for a visible additional contribution of the epoxy lone pair. Thus, in 1Lpe, the HOMO−LUMO transition exhibited $n/\pi \rightarrow \pi^*$ character (Supporting Information Figure S3).

The presence of epoxy groups in the stacked two-layer complex (2L → 2Le) caused a significant qualitative change in the spectrum envelope function. Whereas the 2L complex showed two bands at around 260 and 300 nm, 2Le was characterized by a single wide band at around 290 nm. A qualitatively similar single band spectrum, although more red-shifted, was reported by Wang et al.[42] For the sake of completeness, we note that the maximum peak in the 2Le spectrum was slightly blue-shifted and lower in intensity with respect to 1Lc (strong at 310 nm), the spectrum-dominant constituent of 2Le. Combination of 1Lpe and 2Le generated the 3Le complex, which showed a spectrum qualitatively similar to 2Le. All effects of epoxy groups could clearly be attributed to the lone pair−$\pi$ cloud intermixing and simultaneous reduction of the $sp^2$ conjugated system size. We would like to add here that if epoxy groups are present (see, e.g., refs 1, 4), it makes sense to assume that both types of our CD model spectra (3L and 3Le) may be combined in reality. We theorize that, in such cases, the onset part (spectral range above 300 nm) of the measured absorption spectrum would not possess pure $n \rightarrow \pi^*$ character due to the presence of $\pi \rightarrow \pi^*$ transitions in the same range. Detailed information on the composition of CDs is therefore required in order to allow unambiguous assignments in experimental data.

## CONCLUSIONS

The calculated absorption spectrum of the developed, rather simple, three-layer CD model, consisting of a graphitic core and ∼1.2 nm diameter shell containing oxygen functional groups (i.e., hydrogen-bonded hydroxyl and carboxyl groups within each layer), was consistent with available experimental data. Detailed analysis of its vertical electronic transitions allowed identification of the key characteristics of absorption bands for a large class of carbon dots. Whereas the short-wavelength bands (∼250 nm) were primarily of $\pi \rightarrow \pi^*$ type, the low-energy absorption onset bands at around 300 nm were dominated by interlayer charge transfer with a strong $\pi \rightarrow \pi^*$ component. In the case of the epoxidized CD model, the low-energy onset band contained mixed $n \rightarrow \pi^*$ and interlayer charge transfer transitions. The finding that the low-energy absorption bands contained $\pi \rightarrow \pi^*$ charge transfer contradicts the commonly used $n \rightarrow \pi^*$ textbook assignment. Solvent effects and additional deprotonation did not cause any significant deviations from the gas phase calculations. We showed that theoretical calculations may provide useful information on the absorption spectra of CDs. Single-CD resolved spectroscopy at low temperature combined with precise knowledge on CD composition and supported by theoretical calculations would be desirable to provide ultimate understanding of CD spectra.

## ASSOCIATED CONTENT

### Supporting Information

Interaction and stabilization energies, enthalpies, and Gibbs free energies of two- and three-layer systems; electron density differences in 1Lp, 1Lpe, 1Lc, and 2L; HOMO and LUMO orbital pictures of 1Lp and 1Lpe; absorption spectra of two-layer model conformations; quantification of excitonic coupling in the 2L complex. The Supporting Information is available free of charge on the ACS Publications website at DOI: 10.1021/acs.jpcc.5b04080.

## AUTHOR INFORMATION

### Corresponding Author

*E-mail: michal.otyepka@upol.cz. Phone: +420 585 634 756.

### Notes

The authors declare no competing financial interests.

## ACKNOWLEDGMENTS

Support from the Ministry of Education, Youth and Sports of the Czech Republic (project No. LO1305) is gratefully acknowledged.

## REFERENCES

(1) Zhu, S.; Zhang, J.; Qiao, C.; Tang, S.; Li, Y.; Yuan, W.; Li, B.; Tian, L.; Liu, F.; Hu, R.; et al. Strongly Green-Photoluminescent Graphene Quantum Dots for Bioimaging Applications. *Chem. Commun.* **2011**, *47*, 6858−6860.

(2) Chien, C.-T.; Li, S.-S.; Lai, W.-J.; Yeh, Y.-C.; Chen, H.-A.; Chen, I. S.; Chen, L.-C.; Chen, K.-H.; Nemoto, T.; Isoda, S.; et al. Tunable Photoluminescence from Graphene Oxide. *Angew. Chem., Int. Ed.* **2012**, *51*, 6662−6666.

(3) Dong, Y.; Chen, C.; Zheng, X.; Gao, L.; Cui, Z.; Yang, H.; Guo, C.; Chi, Y.; Li, C. M. One-Step and High Yield Simultaneous Preparation of Single- and Multi-Layer Graphene Quantum Dots from CX-72 Carbon Black. *J. Mater. Chem.* **2012**, *22*, 8764−8766.

(4) Zhang, M.; Bai, L.; Shang, W.; Xie, W.; Ma, H.; Fu, Y.; Fang, D.; Sun, H.; Fan, L.; Han, M.; et al. Facile Synthesis of Water-Soluble, Highly Fluorescent Graphene Quantum Dots as a Robust Biological Label for Stem Cells. *J. Mater. Chem.* **2012**, *22*, 7461−7467.

(5) Jin, S. H.; Kim, D. H.; Jun, G. H.; Hong, S. H.; Jeon, S. Tuning the Photoluminescence of Graphene Quantum Dots through the Charge Transfer Effect of Functional Groups. *ACS Nano* **2013**, *7*, 1239−1245.

(6) Li, L.; Wu, G.; Yang, G.; Peng, J.; Zhao, J.; Zhu, J.-J. Focusing on Luminescent Graphene Quantum Dots: Current Status and Future Perspectives. *Nanoscale* **2013**, *5*, 4015−4039.

(7) Bacon, M.; Bradley, S. J.; Nann, T. Graphene Quantum Dots. *Part. Part. Syst. Charact.* **2014**, *31*, 415−428.

(8) Dreyer, D. R.; Todd, A. D.; Bielawski, C. W. Harnessing the Chemistry of Graphene Oxide. *Chem. Soc. Rev.* **2014**, *43*, 5288−5301.

(9) Wang, L.; Wang, Y.; Xu, T.; Liao, H.; Yao, C.; Liu, Y.; Li, Z.; Chen, Z.; Pan, D.; Sun, L.; et al. Gram-Scale Synthesis of Single-Crystalline Graphene Quantum Dots with Superior Optical Properties. *Nat. Commun.* **2014**, *5*, 5357.



DOI: 10.1021/acs.jpcc.5b04080
*J. Phys. Chem. C* 2015, 119, 13369−13373

(10) Hola, K.; Zhang, Y.; Wang, Y.; Giannelis, E. P.; Zboril, R.; Rogach, A. L. Carbon Dots—Emerging Light Emitters for Bioimaging, Cancer Therapy, and Optoelectronics. *Nano Today* **2014**, *9*, 590−603.
(11) Hola, K.; Bourlinos, A. B.; Kozak, O.; Berka, K.; Siskova, K. M.; Havrdova, M.; Tucek, J.; Safarova, K.; Otyepka, M.; Giannelis, E. P.; et al. Photoluminescence Effects of Graphitic Core Size and Surface Functional Groups in Carbon Dots: $COO^-$ Induced Red-Shift Emission. *Carbon* **2014**, *70*, 279−286.
(12) Kozawa, D.; Zhu, X.; Miyauchi, Y.; Mouri, S.; Ichida, M.; Su, H.; Matsuda, K. Excitonic Photoluminescence from Nanodisc States in Graphene Oxides. *J. Phys. Chem. Lett.* **2014**, *5*, 1754−1759.
(13) Sk, M. A.; Ananthanarayanan, A.; Huang, L.; Lim, K. H.; Chen, P. Revealing the Tunable Photoluminescence Properties of Graphene Quantum Dots. *J. Mater. Chem. C* **2014**, *2*, 6954−6960.
(14) Zhao, M.; Yang, F.; Xue, Y.; Xiao, D.; Guo, Y. A Time-Dependent DFT Study of the Absorption and Fluorescence Properties of Graphene Quantum Dots. *ChemPhysChem* **2014**, *15*, 950−957.
(15) Cowan, D. O.; Drisko, R. L. *Elements of Organic Photochemistry*; Plenum Press: New York, 1976.
(16) Klessinger, M.; Michl, J. *Excited States and Photochemistry of Organic Molecules*; VCH Publishers: New York, 1995.
(17) Bourlinos, A. B.; Zbořil, R.; Petr, J.; Bakandritsos, A.; Krysmann, M.; Giannelis, E. P. Luminescent Surface Quaternized Carbon Dots. *Chem. Mater.* **2012**, *24*, 6−8.
(18) Liu, H.; Ye, T.; Mao, C. Fluorescent Carbon Nanoparticles Derived from Candle Soot. *Angew. Chem., Int. Ed.* **2007**, *46*, 6473−6475.
(19) Ding, C.; Zhu, A.; Tian, Y. Functional Surface Engineering of C-Dots for Fluorescent Biosensing and in Vivo Bioimaging. *Acc. Chem. Res.* **2013**, *47*, 20−30.
(20) Doyle, J. D. *Introduction to Organic Photochemistry*; John Wiley & Sons: New York, 1989.
(21) Luo, Z.; Lu, Y.; Somers, L. A.; Johnson, A. T. C. High Yield Preparation of Macroscopic Graphene Oxide Membranes. *J. Am. Chem. Soc.* **2009**, *131*, 898−899.
(22) Shang, J.; Ma, L.; Li, J.; Ai, W.; Yu, T.; Gurzadyan, G. G. The Origin of Fluorescence from Graphene Oxide. *Sci. Rep.* **2012**, *2*, 792.
(23) Zhang, X.-F.; Shao, X.; Liu, S. Dual Fluorescence of Graphene Oxide: A Time-Resolved Study. *J. Phys. Chem. A* **2012**, *116*, 7308−7313.
(24) Kozawa, D.; Miyauchi, Y.; Mouri, S.; Matsuda, K. Exploring the Origin of Blue and Ultraviolet Fluorescence in Graphene Oxide. *J. Phys. Chem. Lett.* **2013**, *4*, 2035−2040.
(25) Becke, A. D. Density-Functional Thermochemistry. III. The Role of Exact Exchange. *J. Chem. Phys.* **1993**, *98*, 5648−5652.
(26) Grimme, S.; Antony, J.; Ehrlich, S.; Krieg, H. A Consistent and Accurate Ab Initio Parametrization of Density Functional Dispersion Correction (DFT-D) for the 94 Elements H-Pu. *J. Chem. Phys.* **2010**, *132*, 154104.
(27) Chai, J.-D.; Head-Gordon, M. Long-Range Corrected Hybrid Density Functionals with Damped Atom-Atom Dispersion Corrections. *Phys. Chem. Chem. Phys.* **2008**, *10*, 6615−6620.
(28) Jacquemin, D.; Mennucci, B.; Adamo, C. Excited-State Calculations with TD-DFT: From Benchmarks to Simulations in Complex Environments. *Phys. Chem. Chem. Phys.* **2011**, *13*, 16987−16998.
(29) Laurent, A. D.; Jacquemin, D. TD-DFT Benchmarks: A Review. *Int. J. Quantum Chem.* **2013**, *113*, 2019−2039.
(30) Fang, C.; Oruganti, B.; Durbeej, B. How Method-Dependent Are Calculated Differences between Vertical, Adiabatic, and 0−0 Excitation Energies? *J. Phys. Chem. A* **2014**, *118*, 4157−4171.
(31) Barone, V.; Cossi, M. Quantum Calculation of Molecular Energies and Energy Gradients in Solution by a Conductor Solvent Model. *J. Phys. Chem. A* **1998**, *102*, 1995−2001.
(32) Cossi, M.; Rega, N.; Scalmani, G.; Barone, V. Energies, Structures, and Electronic Properties of Molecules in Solution with the C-PCM Solvation Model. *J. Comput. Chem.* **2003**, *24*, 669−681.
(33) Knippenberg, S.; Bohnwagner, M. V.; Harbach, P. H. P.; Dreuw, A. Strong Electronic Coupling Dominates the Absorption and Fluorescence Spectra of Covalently Bound BisBODIPYs. *J. Phys. Chem. A* **2015**, *119*, 1323−1331.
(34) Frisch, M. J.; Trucks, G. W.; Schlegel, H. B.; Scuseria, G. E.; Robb, M. A.; Cheeseman, J. R.; Scalmani, G.; Barone, V.; Mennucci, B.; Petersson, G. A.; et al. *Gaussian 09*, revision D.01; Gaussian, Inc.: Wallingford, CT, 2009.
(35) Shen, R.; Song, K.; Liu, H.; Li, Y.; Liu, H. Dramatic Fluorescence Enhancement of Bare Carbon Dots through Facile Reduction Chemistry. *ChemPhysChem* **2012**, *13*, 3549−3555.
(36) Dong, Y.; Pang, H.; Yang, H. B.; Guo, C.; Shao, J.; Chi, Y.; Li, C. M.; Yu, T. Carbon-Based Dots Co-doped with Nitrogen and Sulfur for High Quantum Yield and Excitation-Independent Emission. *Angew. Chem., Int. Ed.* **2013**, *52*, 7800−7804.
(37) Hu, S.; Tian, R.; Dong, Y.; Yang, J.; Liu, J.; Chang, Q. Modulation and Effects of Surface Groups on Photoluminescence and Photocatalytic Activity of Carbon Dots. *Nanoscale* **2013**, *5*, 11665−11671.
(38) Pan, D.; Zhang, J.; Li, Z.; Wu, M. Hydrothermal Route for Cutting Graphene Sheets into Blue-Luminescent Graphene Quantum Dots. *Adv. Mater.* **2010**, *22*, 734−738.
(39) Li, Y.; Hu, Y.; Zhao, Y.; Shi, G.; Deng, L.; Hou, Y.; Qu, L. An Electrochemical Avenue to Green-Luminescent Graphene Quantum Dots as Potential Electron-Acceptors for Photovoltaics. *Adv. Mater.* **2011**, *23*, 776−780.
(40) Peng, J.; Gao, W.; Gupta, B. K.; Liu, Z.; Romero-Aburto, R.; Ge, L.; Song, L.; Alemany, L. B.; Zhan, X.; Gao, G.; et al. Graphene Quantum Dots Derived from Carbon Fibers. *Nano Lett.* **2012**, *12*, 844−849.
(41) Venugopal, G.; Krishnamoorthy, K.; Mohan, R.; Kim, S.-J. An Investigation of the Electrical Transport Properties of Graphene-Oxide Thin Films. *Mater. Chem. Phys.* **2012**, *132*, 29−33.
(42) Wang, S.; Chen, Z.-G.; Cole, I.; Li, Q. Structural Evolution of Graphene Quantum Dots during Thermal Decomposition of Citric Acid and the Corresponding Photoluminescence. *Carbon* **2015**, *82*, 304−313.


DOI: 10.1021/acs.jpcc.5b04080
*J. Phys. Chem. C* 2015, 119, 13369−13373